

AI-Augmented Density-Driven Optimal Control for Decentralized Environmental Mapping[★]

Kooktae Lee^{*} Julian Martinez^{*}

^{*} Department of Mechanical Engineering, New Mexico Institute of Mining and Technology, Socorro, NM 87801, USA (email: kooktae.lee@nmt.edu / julian.martinez@student.nmt.edu).

Abstract: This paper presents an AI-augmented decentralized framework for multi-agent environmental mapping under limited sensing and communication. While conventional coverage formulations achieve effective spatial allocation when an accurate reference map is available, their performance deteriorates under uncertain or biased priors. The proposed method introduces an adaptive and self-correcting mechanism that enables agents to iteratively refine local density estimates within an optimal transport-based framework, ensuring theoretical consistency and scalability. A dual multilayer perceptron (MLP) module enhances adaptivity by inferring local mean-variance statistics and regulating virtual uncertainty for long-unvisited regions, mitigating stagnation around local minima. Theoretical analysis rigorously proves convergence under the Wasserstein metric, while simulation results demonstrate that the proposed AI-augmented Density-Driven Optimal Control consistently achieves robust and precise alignment with the ground-truth density, yielding substantially higher-fidelity reconstruction of complex multi-modal spatial distributions compared with conventional decentralized baselines.

Keywords: Multi-agent systems, Decentralized control, Non-uniform coverage, Optimal transport, Wasserstein metric, Artificial intelligence, Environmental mapping, Autonomous systems

1. INTRODUCTION

Accurate spatial mapping is essential for autonomous multi-agent systems in applications such as environmental monitoring, pollution tracking, precision agriculture, and disaster response Hollinger and Sukhatme (2014); Binney et al. (2013). In practice, agents must operate under limited sensing, partial communication, and dynamic constraints, while prior environmental knowledge is often sparse or outdated, making it challenging to design decentralized strategies that achieve both efficiency and adaptivity.

Conventional non-uniform coverage frameworks, such as Density-Driven Control (D²C) Afrazi et al. (2025) and its optimal-control extension, Density-Driven Optimal Control (D²OC) Seo and Lee (2025a,b), achieve effective spatial allocation when an accurate reference map is available (see the conceptual illustration in Fig. 1). However, their performance deteriorates when the prior map is uncertain or biased. Other representative approaches, including ergodic exploration Mathew and Mezić (2011); Gkoulelos et al. (2021), information-theoretic coverage Julian et al. (2012), and distributed optimal transport methods Krishnan and Martínez (2025); Bandyopadhyay et al. (2017), also pursue spatially balanced exploration through information- or transport-theoretic formulations. Nevertheless, these methods typically rely on accurate or well-

established priors or globally consistent cost functions, limiting their adaptability under partial sensing and intermittent communication. In realistic environments, however, only coarse and dynamically evolving estimates of the underlying field are available, motivating the need for an adaptive and self-correcting coverage mechanism capable of refining its reference model through continual interaction with noisy observations.

To address these limitations, we propose an AI-augmented decentralized framework in which agents iteratively update local map estimates using online sensing and limited-range communication. This enables progressive reconstruction of the true spatial importance distribution while maintaining adaptive coverage. Unlike conventional informative path planning (IPP) schemes Binney and Sukhatme (2012); Hollinger and Sukhatme (2014), which aim to maximize short-term information gain based on

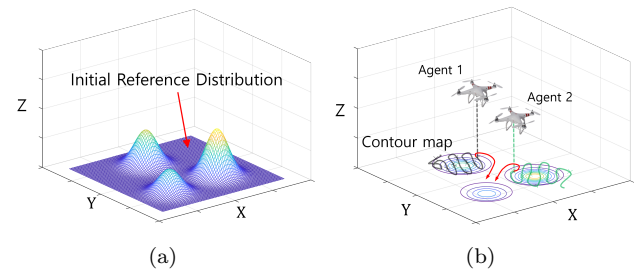


Fig. 1. Conceptual illustration of D²C/D²OC.

[★] This work was supported by NSF CAREER Grant CMMI-DCSD-2145810.

local uncertainty reduction, the proposed framework optimizes a distribution-level objective under the Wasserstein metric, ensuring globally consistent convergence toward the ground-truth density.

The proposed architecture builds upon the D²OC formulation, which ensures mass-preserving updates under the Wasserstein metric for guaranteed convergence. It consists of three stages: (A) sample selection and optimal control, (B) coverage-tracking weight update, and (C) distributed consensus with range-limited communication. This structure supports fully decentralized implementation while maintaining theoretical consistency with optimal transport (OT) principles.

To enhance adaptivity, an AI module is incorporated into Stage A. Each agent employs a dual multilayer perceptron (MLP) inference model: one network provides static mean-variance estimation, while the other dynamically adjusts virtual uncertainty for long-unvisited regions. These learned uncertainty weights modulate local sampling priorities, encouraging re-exploration of neglected areas without centralized coordination. The AI-augmented formulation preserves the analytical structure of D²OC while improving robustness against sensing noise, sample renewal randomness, and local minima.

Unlike previous D²C and D²OC studies that assume a known and accurate reference map, this work addresses the fundamentally different problem of decentralized map reconstruction under uncertain or incomplete priors. The main contributions are summarized as follows: 1) A decentralized framework that reconstructs initially uncertain reference maps through local sensing and neighbor communication without central coordination; 2) Integration of an AI-based dual-MLP inference module into D²OC to guide exploration based on predicted importance and uncertainty; 3) Theoretical proof of convergence under the Wasserstein metric, supported by simulations showing that the AI-augmented D²OC avoids stagnation under biased priors and achieves a significantly lower steady-state Wasserstein distance than the non-AI baseline.

2. PROBLEM DESCRIPTION AND OBJECTIVES

Notations: Let \mathbb{R} denote the set of real numbers, and $\mathbb{N}_0 := \{0, 1, 2, \dots\}$ the set of nonnegative integers. For any vector or matrix, $(\cdot)^\top$ denotes transpose. The discrete-time index is indicated by the superscript $k \in \mathbb{N}_0$, e.g., \mathbf{x}^k represents the state at time step k . The Euclidean norm is denoted by $\|\cdot\|$, and the weighted norm is defined as $\|x\|_R^2 = x^\top Rx$ for a positive-definite matrix $R \succ 0$. The Dirac delta function is denoted by $\delta(\cdot)$. For any set \mathcal{S} , $|\mathcal{S}|$ denotes its cardinality (i.e., the number of elements in \mathcal{S}).

We consider a team of N_a mobile agents operating in a bounded domain $\Omega \subset \mathbb{R}^d$. The true spatial importance of each point $x \in \Omega$ is represented by an unknown distribution ρ_{GT} , indicating the priority of monitoring that region. In practice, agents initially possess only a coarse prior map $\hat{\rho}$ from historical or low-fidelity data, and must therefore *explore the environment while refining their local estimates* to approximate ρ_{GT} .

Each agent i maintains a local *sample-based reference map*:

$$\hat{\rho}_i^k(x) = \sum_{j=1}^{N_s} w_j^k \delta(x - q_j^k), \quad (1)$$

where N_s is the number of sample points, $q_j^k \in \Omega$ denotes the j th sample location, and w_j^k its associated weight. Weights represent local importance inferred from sensing and are updated via communication with nearby agents. All computations are fully decentralized without any global fusion.

To ensure energy-aware exploration, each agent limits its operation to a finite set of discrete points M , determined by its operation time T_{op} and sampling interval Δt , i.e., $M = T_{\text{op}}/\Delta t$. Each agent point is associated with a normalized mass $1/M$, and the sample weights satisfy $\sum_j w_j^k = 1$, defining the empirical distribution $\hat{\rho}_i^k$ that evolves as exploration proceeds.

The objective is to minimize the discrepancy between each agent's local map $\hat{\rho}_i^k(x)$ and the ground-truth density $\rho_{\text{GT}}(x)$, measured by the 2-Wasserstein distance:

$$\mathcal{W}_2^2(\hat{\rho}_i^k, \rho_{\text{GT}}) = \min_{\pi \in \Pi(\hat{\rho}_i^k, \rho_{\text{GT}})} \sum_{i,j} \pi_{ij} \|p_i - q_j\|^2, \quad (2)$$

where $\Pi(\hat{\rho}_i^k, \rho_{\text{GT}})$ denotes feasible transport plans $\pi_{ij} \geq 0$ satisfying $\sum_j \pi_{ij} = 1/M$ and $\sum_i \pi_{ij} = w_j$.

We aim to design decentralized update rules and control inputs such that

$$\lim_{k \rightarrow \infty} \mathcal{W}_2(\hat{\rho}_i^k, \rho_{\text{GT}}) \leq \epsilon, \quad \forall i, \quad (3)$$

where ϵ is a small residual error due to finite sampling.

While classical OT seeks the optimal transport plan π_{ij} minimizing (2) for fixed point sets $\{p_i\}$ and $\{q_j\}$, the proposed D²OC framework instead determines the *control-driven sequence of $\{p_i^k\}$* that gradually reduces this distance, which is an inherently much more challenging problem.

Conceptually, this involves two coupled objectives:

- (1) **Adaptive coverage:** Agents move so that their collective trajectories are proportional to the estimated importance distribution, prioritizing high-value regions.
- (2) **Incremental map refinement:** As agents sense new data, they update the sample weights w_j^k , improving local map fidelity and guiding subsequent motions.

The coupling can be formalized by the time-averaged empirical measure:

$$\hat{\rho}_{i,\text{agent}}^K(x) = \frac{1}{K} \sum_{k=1}^K \delta(x - p_i^k), \quad (4)$$

where p_i^k is the agent's position at step k . Accurate mapping is achieved when $\hat{\rho}_{i,\text{agent}}^K(x)$ matches $\hat{\rho}_i^k(x)$, which in turn converges toward ρ_{GT} via iterative weight and sample updates. Thus, motion and weight adaptation jointly minimize the Wasserstein distance between the empirical $\hat{\rho}$ and true distributions ρ_{GT} .

In practice, the decentralized D²OC framework Seo and Lee (2025b) proceeds in three stages (A–C): agents compute local centroids for motion, update sample weights, and exchange information with neighbors. Unlike the original D²OC formulation, which assumes that the reference distribution is perfectly known *a priori* and does not require sensing-based updates, the proposed AI-augmented framework newly incorporates an inference mechanism that estimates uncertainty in unobserved regions and pri-

oritizes sampling. This extension enables D²OC to operate under realistic conditions where the true distribution is initially unknown and must be progressively inferred through exploration.

The overall goal is thus to design *decentralized iterative rules for motion and weight updates* so that each local map $\hat{\rho}_i^k(x)$ converges to ρ_{GT} in Wasserstein distance, while collective trajectories realize non-uniform coverage aligned with the evolving map. This formulation motivates the subsequent development of the control mechanism, AI inference, and convergence analysis.

3. DECENTRALIZED DENSITY-DRIVEN OPTIMAL CONTROL

This section formulates the proposed AI-augmented D²OC framework for decentralized multi-agent coverage in environments with unknown or imperfectly estimated spatial importance distributions.

Before executing control updates, each agent renews its reference sample set through a *Dynamic Sample Generation and Removal* process. The main procedure then consists of three stages: *Stage A: Sample Selection & Optimal Control*, *Stage B: Weight Update*, and *Stage C: Communication & Merging*. An AI-based module estimates sample uncertainty for computing priority scores, as detailed in Section 4.

3.1 Dynamic Sample Generation and Removal

Before the control update in Stage A, each agent renews its sample set $\mathcal{S}_i^k = \{q_j^k\}$ based on recent sensory measurements. At each step, agent i explores its neighborhood within a sensing range r_s and generates candidate samples according to the measured field intensity. Each candidate location x_j^k within the sensing range is evaluated through a noisy sensing model

$$\xi_j^k = \rho_{\text{GT}}(x_j^k) + \varepsilon_j^k, \quad \varepsilon_j^k \sim \mathcal{N}(0, \sigma_{\text{sensor}}^2),$$

where ξ_j^k denotes the instantaneous sensor reading. From accumulated measurements and neighborhood statistics, the local mean μ_j^k and variance $(\sigma_j^k)^2$ are estimated, representing the agent's belief about the field intensity at x_j^k . Candidates with higher measured values are retained and added as new samples q_j^k to the reference set. Accepted points are initialized with nominal weights and variances, forming the newly born subset of \mathcal{S}_i^k .

Meanwhile, existing samples within the sensing region are examined for removal. If their field intensity falls below a distance-dependent threshold, they are discarded, representing the death process. This *birth–death* mechanism continuously adapts the reference distribution $\{q_j\}$ to new sensory information, maintaining a concise and up-to-date sample representation for subsequent control-driven redistribution in Stage A.

3.2 Stage A: Sample Selection and Optimal Control

Let $p_i^k \in \mathbb{R}^d$ denote the position of agent i at time k . Each sample $q_j^k \in \mathcal{S}_i^k$ is assigned an *importance score*

$$\phi_j^k = \mu_j^k + c_1(\sigma_j^k)^2 + c_2(\sigma_{j,\text{virtual}}^k)^2, \quad (5)$$

where c_1, c_2 are some positive coefficients, μ_j^k and $(\sigma_j^k)^2$ are the locally measured mean and variance obtained from sensor feedback at step k , and $(\sigma_{j,\text{virtual}}^k)^2$ is an auxiliary variance adaptively estimated by a separate AI module to encourage exploration of long-unvisited regions. Two distinct neural modules are employed in practice: one refines the measured statistics (μ_j^k, σ_j^k) to suppress sensor noise, while the other updates $\sigma_{j,\text{virtual}}^k$ online based on the agent's visitation history. The combined score balances reliable exploitation of informative regions (μ_j^k, σ_j^k) with active exploration driven by the virtual uncertainty term. This importance score is then used in the weighted centroid computation of Stage A to determine each agent's next reference position.

The *score* of each sample balances importance and proximity $s_j^k = \frac{\phi_j^k}{\|p_i^k - q_j^k\|}$. Samples are sorted in descending order of s_j^k , and selected sequentially until the cumulative weight reaches the agent's total mass budget $1/M$: $\sum_{j \in \mathcal{S}_{i,\text{loc}}^k} w_j = \frac{1}{M}$. The resulting subset $\mathcal{S}_{i,\text{loc}}^k$ represents the locally influential samples that participate in the optimal control update for agent i .

Optimal Control Formulation: Each agent follows discrete-time LTI dynamics:

$$\mathbf{x}_i^{k+1} = A_i \mathbf{x}_i^k + B_i u_i^k, \quad p_i^k = C_i \mathbf{x}_i^k, \quad (6)$$

where $A_i \in \mathbb{R}^{n \times n}$, $B_i \in \mathbb{R}^{n \times m}$, and $C_i \in \mathbb{R}^{d \times n}$ are the system matrices of agent i , and $u_i^k \in \mathbb{R}^m$ denotes the control input at time k .

The finite-horizon optimal control problem minimizes the cumulative transport and control effort over a planning horizon H :

$$J_i(u_i^{k:k+H-1}) = \sum_{l=k}^{k+H} \sum_{j \in \mathcal{S}_{i,\text{loc}}^l} \pi_{lj}^* \|p_i^{l+1} - q_j^k\|^2 + \sum_{l=k}^{k+H} \|u_i^l\|_R^2, \quad (7)$$

subject to the discrete-time LTI dynamics in (6), where H is the prediction horizon, π_{lj}^* denotes the optimal transport plan with an analytic solution available in Kabir and Lee (2021), $\mathcal{S}_{i,\text{loc}}^l$ is the local sample set at step l , and $R \succ 0$ is the control weighting matrix. Here, the first term denotes the local Wasserstein distance and the second term reflects the input penalty.

Optimal Control via Weighted Centroid: For each agent i , let $\mathcal{S}_{i,\text{loc}}^l$ denote the set of selected samples at discrete time l and π_{lj}^* be the transport weight associated with each sample $q_j^k \in \mathcal{S}_{i,\text{loc}}^l$. Define the weighted centroid of the selected samples for agent i at time l as

$$q_{i,c}^l = \sum_{j \in \mathcal{S}_{i,\text{loc}}^l} \pi_{lj}^* q_j^k / \sum_{j \in \mathcal{S}_{i,\text{loc}}^l} \pi_{lj}^* \quad (8)$$

Then, the following result holds.

Lemma 1. (Weighted centroid minimizes the local quadratic cost). For agent i at step l , consider

$$J_{i,\text{dist}}^l = \sum_{j \in \mathcal{S}_{i,\text{loc}}^l} \pi_{lj}^* \|p_i^{l+1} - q_j^k\|^2,$$

where $\pi_{lj}^* \geq 0$ denote the optimal transport coefficients. Let $\gamma_l := \sum_{j \in \mathcal{S}_{i,\text{loc}}^l} \pi_{lj}^*$ and $q_{i,c}^l := \frac{1}{\gamma_l} \sum_{j \in \mathcal{S}_{i,\text{loc}}^l} \pi_{lj}^* q_j^k$. Then $J_{i,\text{dist}}^l$ is minimized by $p_i^{l+1} = q_{i,c}^l$.

Proof 1. Using the standard identity for weighted squared distances, $\sum_j \pi_{lj}^* \|p_i^{l+1} - q_j^l\|^2 = \gamma_l \|p_i^{l+1} - q_{i,c}^l\|^2 + \sum_j \pi_{lj}^* \|q_j^l - q_{i,c}^l\|^2$, where $\gamma_l = \sum_j \pi_{lj}^*$. The second term is independent of p_i^{l+1} , so the minimum is attained at $p_i^{l+1} = q_{i,c}^l$. Since the centroid is recomputed at every control step, this property holds sequentially across the H -step horizon, ensuring local optimality at each stage.

Optimal Control under Discrete-Time LTI Dynamics: The previous lemma characterizes the instantaneous optimal position update that minimizes the local quadratic cost. In a more realistic setting, however, agent motion is constrained by discrete-time linear dynamics. We therefore extend this result to derive a closed-form control law that optimally drives each agent toward its weighted centroid over a finite prediction horizon.

Theorem 1. (Analytic Receding-Horizon Control Law in D²OC) Consider agent i with discrete-time LTI dynamics (6) and the stage cost induced by (7) at step l . Let the weighted centroid of $\mathcal{S}_{i,\text{loc}}^l$ be defined in (8) with $\gamma_l := \sum_{j \in \mathcal{S}_{i,\text{loc}}^l} \pi_{lj}^*$. Then the control input that minimizes the stage cost at step l is

$$u_i^l = (R + \gamma_l B_i^\top B_i)^{-1} \gamma_l B_i^\top (q_{i,c}^l - A_i \mathbf{x}_i^l), \quad (9)$$

$$l = k, \dots, k+H-1.$$

Applying this stepwise for $l = k, \dots, k+H-1$ yields a receding-horizon control law consistent with the H -step cost.

Proof 2. At each step l , the instantaneous stage cost can be written as $\tilde{J}_i^l = \sum_{j \in \mathcal{S}_{i,\text{loc}}^l} \pi_{lj}^* \|A_i \mathbf{x}_i^l + B_i u_i^l - q_j^l\|^2 + (u_i^l)^\top R u_i^l$. The first term quantifies the transport discrepancy between the propagated agent position and the nearby samples selected at step l , while the second term penalizes control energy to prevent excessive maneuvers. Here, π_{lj}^* represents the portion of mass transported from the agent's next predicted position to each sample q_j^l , establishing a direct coupling between optimal transport and control.

Applying the weighted-distance decomposition yields $\sum_j \pi_{lj}^* \|A_i \mathbf{x}_i^l + B_i u_i^l - q_j^l\|^2 = \gamma_l \|A_i \mathbf{x}_i^l + B_i u_i^l - q_{i,c}^l\|^2 + \sum_j \pi_{lj}^* \|q_j^l - q_{i,c}^l\|^2$, where $\gamma_l = \sum_{j \in \mathcal{S}_{i,\text{loc}}^l} \pi_{lj}^*$ is the total transported mass. The second term is independent of u_i^l and thus does not affect the minimizer. Minimizing \tilde{J}_i^l is therefore equivalent to minimizing

$$\hat{J}_i^l = \gamma_l \|A_i \mathbf{x}_i^l + B_i u_i^l - q_{i,c}^l\|^2 + (u_i^l)^\top R u_i^l.$$

This formulation reveals a quadratic trade-off between tracking accuracy (through centroid alignment) and actuation cost (through the control penalty).

Taking the gradient with respect to u_i^l and setting it to zero gives

$$\nabla_{u_i^l} \hat{J}_i^l = 2\gamma_l B_i^\top (A_i \mathbf{x}_i^l + B_i u_i^l - q_{i,c}^l) + 2R u_i^l = 0,$$

which leads to $(R + \gamma_l B_i^\top B_i) u_i^l = \gamma_l B_i^\top (q_{i,c}^l - A_i \mathbf{x}_i^l)$. Solving for u_i^l yields the analytic form in (9). Since the horizon cost is additive and the centroid is updated at each step, applying the one-step optimizer sequentially provides a stagewise implementation of the finite-horizon control law.

3.3 Stage B: Coverage-Tracking Weight Update

After each motion step, each agent updates its local sample weights to reflect the accumulated coverage of the surrounding region. This operation does not physically transport mass but serves as a *coverage-tracking step* that records local exploration. Consequently, samples in frequently visited areas lose influence, while those in rarely visited regions retain higher importance. The total empirical mass is strictly preserved, ensuring consistency with the D²OC conservation property.

Let $d_{ij}^k = \|p_i^k - q_j^k\|$ denote the distance between agent i and sample q_j^k . Samples closer to the agent are assigned higher removal priority as

$$r_j = \frac{d_{ij}^k}{1 + \beta((\sigma_j^k)^2 + (\sigma_{j,\text{virtual}}^k)^2)}, \quad (10)$$

where $\beta > 0$ balances spatial proximity and uncertainty. Here, σ_j^k is the intrinsic sensing variance, and $\sigma_{j,\text{virtual}}^k$ is the AI-adapted exploration variance.

Let $\mathcal{Q}_i^k \subseteq \mathcal{S}_i^k$ denote the subset of samples selected for weight reduction in ascending order of (10), such that their cumulative decrease satisfies

$$\sum_{j \in \mathcal{Q}_i^k} (w_j^k - w_j^{k+1}) = \frac{1}{M}. \quad (11)$$

This update quantifies cumulative coverage progress while preserving total mass and preventing numerical drift.

3.4 Stage C: Communication and Merging

At each iteration, agents exchange their locally maintained sample sets with nearby peers within the communication range r_c . The neighbor set of agent i at step k is defined as

$$\mathcal{N}_i^k = \{j \mid \|p_i^k - p_j^k\| \leq r_c\}, \quad (12)$$

and information exchange occurs only among such neighboring pairs.

Through local communication, each agent gathers the sample sets of its neighbors $\{\mathcal{S}_j^k \mid j \in \mathcal{N}_i^k\}$ and merges them with its own set \mathcal{S}_i^k . Spatially redundant samples are unified based on positional proximity, and the merged set is downsampled to maintain a fixed size N using a farthest-point selection strategy Li et al. (2022). This guarantees that each agent preserves a compact yet diverse representation of the collective sampling history without unbounded growth in memory.

After merging, the sample weights are projected back to the feasible set of nonnegative measures to preserve mass consistency: $w_j^{k+1} \geq 0, \sum_j w_j^{k+1} = \sum_j w_j^k$. (13)

This procedure guarantees that each agent maintains a bounded yet informative local representation of the environment.

Remark 1. (Role of Stage C in Decentralized Consensus). Stage C functions as the decentralized consensus layer of the framework. Through limited-range exchanges, agents reconcile their local sample representations to maintain globally consistent mapping and coverage information. This enables coherent control updates across the network even under partial communication and asynchronous operation.

4. DUAL-MLP INFERENCE FOR MEAN–VARIANCE AND ADAPTIVE UNCERTAINTY ESTIMATION

To guide decentralized multi-agent exploration, two neural networks (MLPs) estimate statistical properties of candidate samples. The first refines the locally measured mean and variance of the environmental field, while the second adaptively updates a *virtual* variance reflecting how long a region has been unvisited. Together, these modules provide complementary exploitation and exploration cues without altering the core D²OC control framework.

4.1 Dual-MLP Architecture

The framework employs two independent MLPs.

MLP-MeanVar: predicts local mean μ_j^k and intrinsic variance $(\sigma_j^k)^2$ for samples $q_j^k \in \mathcal{S}_i^k$. Inputs include the sample coordinates q_j^k , agent state p_i^k (and optionally velocity), historical observations, and neighborhood statistics. The network consists of two hidden layers with 64 neurons each and employs Rectified Linear Unit activations, $\text{ReLU}(x) = \max(0, x)$. It outputs a two-dimensional vector $y_j^k = [\mu_j^k, \log(\sigma_j^k)^2]$, where representing the variance in logarithmic form ensures numerical stability and positivity. The predicted statistics are then substituted into the importance score (5), which is used in Stage A for centroid computation. This network operates in inference mode only, with no online training.

MLP-AdaptiveStd: updates the virtual variance $\sigma_{j,\text{virtual}}^k$ through online learning to promote exploration. Its input concatenates the sample feature z_j^k and the current $\sigma_{j,\text{virtual}}^k$, and the output is the increment $\Delta\sigma_{j,\text{virtual}}^k$. It shares the same layer structure as MLP-MeanVar but has a single output neuron. This network is trained online prior to Stage B, so that long-unvisited samples receive larger virtual variance and thus reduced removal priority in (10).

4.2 Integration with D²OC

Sample Scoring and Weight Redistribution: Both Stage A and Stage B use the same importance score ϕ_j^k . In Stage A, it determines the weighted centroid guiding agent motion toward informative or uncertain regions. In Stage B, the same score appears in the removal priority in (10) so that regions with high total uncertainty retain mass longer, promoting balanced coverage. This unified formulation maintains consistent exploration–exploitation trade-offs while preserving local mass conservation.

4.3 Online Learning Procedure for Dual MLPs

Both MLPs operate over the entire sample set \mathcal{S}_i^k maintained by each agent. The first network (MLP-MeanVar) serves as a fixed regressor providing $(\mu_j^k, (\sigma_j^k)^2)$ for each sample, which can be pre-trained or replaced by user-defined parameters depending on the experimental setup. The second network (MLP-AdaptiveStd) is updated online before Stage B using visitation history and recent measurements to estimate a virtual uncertainty term for long-unvisited or newly generated samples. This additional term is combined with the baseline variance in both

Stage A’s centroid computation and Stage B’s redistribution priority.

Forward Computation: For the L -layer MLP-MeanVar, the forward pass is defined as

$$h^{(0)} = x_j, \quad y_j = W^{(L)}h^{(L-1)} + b^{(L)} = [\mu_j^k, \log(\sigma_j^k)^2]^\top, \\ h^{(l)} = \psi(W^{(l)}h^{(l-1)} + b^{(l)}), \quad l = 1, \dots, L-1,$$

where x_j includes the spatial coordinates q_j^k , agent state, and historical sensor measurements. The activation $\psi(\cdot)$ is ReLU, $\psi(x) = \max(0, x)$. The logarithmic form ensures numerical stability and positivity of the predicted variance.

Similarly, for MLP-AdaptiveStd,

$$z_j^{(0)} = [q_j^k; \sigma_{j,\text{virtual}}^k], \quad \Delta\sigma_j = V^{(L)}z^{(L-1)} + c^{(L)}, \\ z_j^{(l)} = \psi(V^{(l)}z^{(l-1)} + c^{(l)}), \quad l = 1, \dots, L-1,$$

where the input concatenates the sample feature with its current virtual variance. The output $\Delta\sigma_j$ is applied to update the virtual variance as

$$\sigma_{j,\text{virtual}}^{k+1} = \sigma_{j,\text{virtual}}^k + \Delta\sigma_j.$$

Loss Function: Since MLP-MeanVar operates only in inference mode, no loss is computed for it. MLP-AdaptiveStd, however, minimizes a simple regularization loss:

$$\mathcal{L}_{\text{AdaptiveStd}} = \frac{1}{|\mathcal{S}_i^k|} \sum_{q_j^k \in \mathcal{S}_i^k} (\Delta\sigma_{j,\text{virtual}} - \Delta\sigma_{\text{target}})^2.$$

This loss enforces stability by minimizing unnecessary changes in the virtual standard deviation. The target value $\Delta\sigma_{\text{target}} = 0$ is chosen as the nominal per-step behavior, i.e., if a sample is being sensed regularly, its virtual uncertainty should not keep growing. In other words, no further inflation of $\sigma_{j,\text{virtual}}$ is desired in the well-observed (steady-state) case. Only long-unvisited samples, detected through the online update rule, produce nonzero increments, whereas frequently visited ones remain nearly unchanged.

Parameter Update: After computing $\mathcal{L}_{\text{AdaptiveStd}}$ at step k , the network parameters are updated using a gradient-descent rule:

$$\theta_{\text{AdaptiveStd}}^{k+1} = \theta_{\text{AdaptiveStd}}^k - \eta \nabla_{\theta_{\text{AdaptiveStd}}} \mathcal{L}_{\text{AdaptiveStd}},$$

where $\eta > 0$ denotes the learning rate. The updated parameters are then used in the subsequent control step $k+1$ to predict

$$\Delta\sigma_{j,\text{virtual}}^{k+1} = f_{\text{AdaptiveStd}}(q_j^k, p_i^{k+1}; \theta_{\text{AdaptiveStd}}^{k+1}).$$

Algorithmic Summary: At each control step k , the following procedure is executed:

- (1) Measure local field values and compute empirical $\hat{\mu}_j$, $\hat{\sigma}_j^2$.
- (2) Predict $(\mu_j^k, (\sigma_j^k)^2)$ via the fixed MLP-MeanVar.
- (3) Compute $\Delta\sigma_{j,\text{virtual}}$ via MLP-AdaptiveStd and update $\sigma_{j,\text{virtual}}^{k+1} = \sigma_{j,\text{virtual}}^k + \Delta\sigma_{j,\text{virtual}}$.
- (4) Compute the loss $\mathcal{L}_{\text{AdaptiveStd}}$ and update parameters using backpropagation.
- (5) Proceed to Stages A and B using updated virtual variances and predicted means/variances.

Remark 2. (Dual-Network Roles and Advantages). The dual-network design separates static inference from adaptive learning. MLP-MeanVar provides stable baseline statistics for environmental reconstruction, while MLP-Adaptive Std continuously refines exploration bias through online updates. This separation maintains a clear distinction between intrinsic field uncertainty and exploration-induced virtual uncertainty, achieving a stable exploration-exploitation balance within the decentralized D²OC framework.

5. CONVERGENCE ANALYSIS

This section establishes that the iterative execution of the sensor-driven renewal and Stages A–C in the proposed D²OC framework drives the empirical distribution $\hat{\rho}$ toward the ground-truth density ρ_{GT} in the Wasserstein sense. At each control step, agents locally minimize the quadratic cost (7) by moving toward their weighted centroids (8), while the renewal process dynamically adds or removes samples based on the sensed field intensity. This continual update of sample weights refines $\hat{\rho}$ around ρ_{GT} as the environment is progressively explored. The overall evolution of $\hat{\rho}$ thus combines optimal local motion, bounded auxiliary adjustment, and intermittent consensus among neighboring agents. Under these coupled dynamics, the following convergence property holds.

Theorem 2. (Band-Limited Convergence of AI-Augmented D²OC). Consider N_a agents evolving under the discrete-time LTI dynamics (6). Agent i at step k maintains an empirical, nonstationary measure

$$\hat{\rho}_i^k = \sum_j w_j^k \delta(x - q_j^k), \quad \hat{\rho}^k = \frac{1}{N_a} \sum_{i=1}^{N_a} \hat{\rho}_i^k.$$

The measure $\hat{\rho}^k$ is updated at each step by the D²OC control loop, consisting of a sensor-driven renewal (pre-update) and the control–communication stages (A–C).

Assume the following conditions hold:

- (1) **Pre-update (Dynamic sample generation and removal).** Before each control update, every agent renews its local sample set using new sensor feedback. High-value regions generate new samples, while those whose field intensity falls below a distance-dependent threshold are removed. This birth–death renewal perturbs the empirical distribution by a uniformly bounded amount, referred to as the *renewal disturbance*, satisfying $\varepsilon_{\text{renew}} > 0$.
- (2) **Stage A (Local optimal control).** Each agent applies the analytic optimal control (9) derived in Theorem 1, producing a contractive update in the Wasserstein metric.
- (3) **Stage B (Coverage-Tracking redistribution).** After the motion update, each agent redistributes its sample weights to represent how much of the surrounding region has been explored. The redistribution priority follows (10), where $\beta > 0$ balances spatial proximity and combined uncertainty. The total empirical mass of each agent remains exactly conserved, i.e., $\sum_{j \in \mathcal{Q}_i^k} w_j^{k+1} = \sum_{j \in \mathcal{Q}_i^k} w_j^k = 1/M$. This step reassigns existing weights without creating new mass and therefore introduces no additional disturbance to convergence.

(4) **Stage C (Intermittent consensus).** Communication occurs over a jointly connected graph, guaranteeing that local empirical measures asymptotically agree in expectation.

Then, there exist constants $0 < \underline{\mathcal{W}} \leq \bar{\mathcal{W}}$ such that the nonstationary empirical distribution satisfies

$$\underline{\mathcal{W}} \leq \liminf_{k \rightarrow \infty} \mathcal{W}_2(\hat{\rho}^k, \rho_{\text{GT}}) \leq \limsup_{k \rightarrow \infty} \mathcal{W}_2(\hat{\rho}^k, \rho_{\text{GT}}) \leq \bar{\mathcal{W}},$$

where $\bar{\mathcal{W}} = \frac{\varepsilon_{\text{renew}}}{1-\gamma_A}$ and $\underline{\mathcal{W}} > 0$, with $\varepsilon_{\text{renew}} > 0$ denoting the uniformly bounded disturbance introduced by the sensor-driven renewal step and $0 < \gamma_A < 1$ representing the contraction rate of the local control mapping.

Proof 3. Let \mathcal{T}_R , \mathcal{T}_A , \mathcal{T}_B , and \mathcal{T}_C denote, respectively, the update mappings corresponding to (i) sensor-driven renewal, (ii) local optimal control, (iii) coverage-tracking redistribution, and (iv) intermittent consensus.

1) *Renewal step (sample birth-and-death).* Each agent renews its sample set based on sensor feedback: new samples are generated near high-GT regions and low-value ones are discarded according to a distance-dependent threshold. Because sensing is recurrent and both sensor noise and update radii are bounded, the induced perturbation on the empirical distribution is also uniformly bounded:

$$\mathcal{W}_2(\mathcal{T}_R(\hat{\rho}^k), \rho_{\text{GT}}) \leq \mathcal{W}_2(\hat{\rho}^k, \rho_{\text{GT}}) + \varepsilon_{\text{renew}}, \quad \varepsilon_{\text{renew}} > 0.$$

2) *Stage A: contraction through local optimal control.*

At step k , agent i solves the H -step cost (7), where the weighted centroid (8) is computed from the updated samples in $\hat{\rho}_i^k$. The analytic optimal control (9) from Theorem 1 yields

$$\mathbf{x}_i^{l+1} = F_l \mathbf{x}_i^l + G_l q_{i,c}^l, \quad F_l = A_i - B_i (R + \gamma_l B_i^\top B_i)^{-1} \gamma_l B_i^\top A_i.$$

If F_l is Schur-stable ($R \succ 0$, moderate γ_l), the mapping \mathcal{T}_A is contractive in \mathcal{W}_2 :

$$\mathcal{W}_2(\mathcal{T}_A(\hat{\rho}^k), \rho_{\text{GT}}) \leq \gamma_A \mathcal{W}_2(\hat{\rho}^k, \rho_{\text{GT}}), \quad 0 < \gamma_A < 1.$$

3) *Stage B: coverage-tracking redistribution.* After motion, each agent redistributes its sample weights according to the priority r_j^k while keeping $\sum_{j \in \mathcal{Q}_i^k} w_j^{k+1} = \sum_{j \in \mathcal{Q}_i^k} w_j^k = 1/M$. Since this process merely redistributes fixed mass over existing samples, it is nonexpansive in \mathcal{W}_2 and introduces no additional disturbance:

$$\mathcal{W}_2(\mathcal{T}_B(\hat{\rho}^k), \rho_{\text{GT}}) \leq \mathcal{W}_2(\hat{\rho}^k, \rho_{\text{GT}}).$$

4) *Stage C: intermittent consensus.* Agents communicate only within range r_c , forming a time-varying graph \mathcal{G}^k with averaging matrix $A^k = [a_{il}^k]$. Under joint connectivity, the sequence $\{A^k\}$ is ergodic Moreau (2005), ensuring

$$\mathbb{E}[\mathcal{W}_2(\hat{\rho}_i^k, \hat{\rho}_\ell^k)] \rightarrow 0, \quad \forall i, \ell,$$

thus \mathcal{T}_C is mean-nonexpansive in \mathcal{W}_2 .

5) *Composite inequality.* Combining the mappings yields

$$\mathcal{W}_2(\hat{\rho}^{k+1}, \rho_{\text{GT}}) \leq \gamma_A \mathcal{W}_2(\hat{\rho}^k, \rho_{\text{GT}}) + \varepsilon_{\text{renew}}.$$

Iterating gives

$$\limsup_{k \rightarrow \infty} \mathcal{W}_2(\hat{\rho}^k, \rho_{\text{GT}}) \leq \frac{\varepsilon_{\text{renew}}}{1-\gamma_A} =: \bar{\mathcal{W}}.$$

6) *Positive error floor.* Since $\hat{\rho}^k$ is a finite-sample approximation of continuous ρ_{GT} , a nonzero mismatch remains:

$$\liminf_{k \rightarrow \infty} \mathcal{W}_2(\hat{\rho}^k, \rho_{\text{GT}}) \geq \underline{\mathcal{W}} > 0,$$

so ρ^k converges within $[\mathcal{W}, \bar{\mathcal{W}}]$, limited by finite-sample and renewal errors.

Remark 3. (On the necessity of dual MLPs). The convergence in Theorem 2 holds for the AI-augmented D²OC, where the dual MLPs ensure that Stage A remains contractive in practice. Without these AI modules, the control update may lose its contraction property since agents may stagnate near locally dense regions, and the Wasserstein distance stops decreasing, violating the assumed $\gamma_A < 1$ condition. Hence, the *MLP-MeanVar* and *MLP-AdaptiveStd* are essential not for tightening the theoretical bound itself but for realizing the contraction behavior that the theorem presumes.

6. SIMULATIONS

To evaluate the proposed AI-augmented D²OC framework, we performed simulations under a representative abstraction of a *landfill methane plume detection* scenario. Detecting small and transient methane plumes is inherently challenging since satellite-based sensing often fails to distinguish weak emission signals from background variations due to limited spatial resolution and atmospheric scattering Rouet-Leduc and Hulbert (2024). In contrast, UAV- or ground-based sensing offers higher accuracy but is constrained by flight time, sensing range, and intermittent communication Shaw et al. (2021). The simulation environment captures these essential characteristics, multiple localized emission sources, limited sensing range, and communication constraints, allowing systematic evaluation of the algorithm's adaptability and convergence across diverse environmental mapping conditions.

6.1 Simulation Setup

The simulation parameters used in this study are summarized in Table 1. These parameters define a 200×200 m² domain, AI training configuration, and quadrotor dynamic limits, representing a realistic mid-scale environment suitable for validation of decentralized mapping performance.

In Fig. 2(a), the simulated landfill gas mapping environment is illustrated. The red-shaded region represents the ground-truth (GT) plume distribution, which is unknown to the multi-agent system, while five linearized quadrotors are deployed as robotic platforms. The blue dots indicate the initial sample distribution, representing the system's prior estimate of the plume distribution. Even if such prior information is unavailable, the proposed method can flexibly operate using a uniform reference distribution as a baseline. As shown in Fig. 2, the reference samples are deviated from the GT to provide an initial estimation error on purpose.

6.2 Result Analysis

Figs. 2(b,c) illustrate the multi-agent trajectories under two control strategies: (b) D²OC without MLP and (c) AI-augmented D²OC with MLP. The initial and final positions of the five agents are shown by orange circles and magenta squares, respectively. The optimal control inputs are obtained using Theorem 1 with horizon $H = 5$. In simulation, input bounds on velocity and attitude rates are

Table 1. Simulation Parameters

Parameter	Value (Unit)
Domain Size	200×200 (m ²)
Sample Size (N_s)	300 (-)
Sampling Interval (Δt)	0.2 (s)
Number of Agents (N_a)	5 (-)
Operation Time (T_{op})	600 (s) = 10 (mins)
Total Control Steps (M)	3000 (-)
Sensing/Comm. Range (r_s/r_c)	10 (m)/20 (m)
Sample Create/Drop Thresholds	1×10^{-5} (-)/ 2×10^{-6} (-)
Uncertainty Weights (c_1/c_2)	1.0 (-)/1.0 (-)
Trade-off weight (β)	1.0 (-)
Horizon (H) / Input Weight (R)	5 (-) / $0.01I_2$ (-)
Max Vel/Max Tilt/Angular Rate	5 (m/s)/10 (°)/30 (°/s)
Hidden Layers/Neurons per Layer	2 (-)/64 (-)
Learning Rate (η)	1×10^{-3} (-)
MLP Update Interval (T_{MLP})	10 (step)

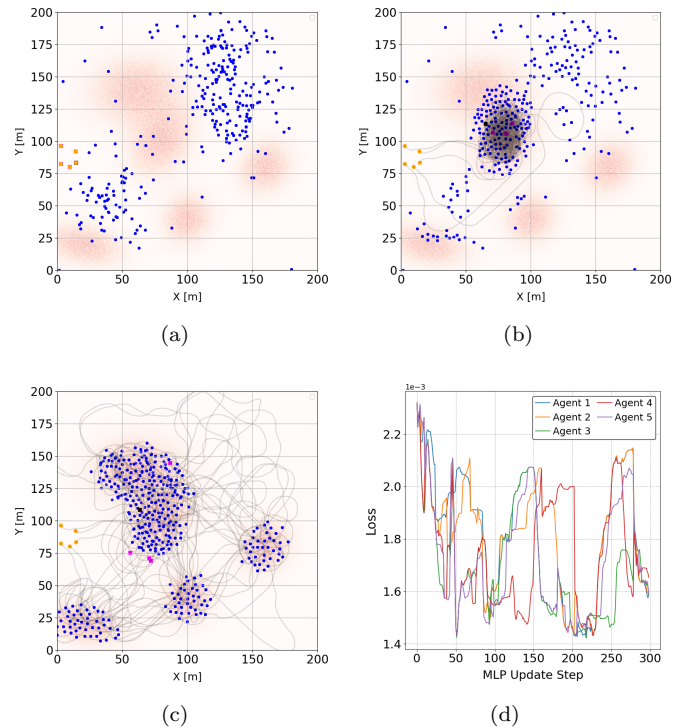


Fig. 2. Simulation results: (a) Initial reference samples (blue), GT distribution (shaded red), and initial positions of five agents; (b) Updated sample distribution after mission completion without AI augmentation; (c) Results of AI-augmented D²OC showing improved coverage efficiency compared to (b); (d) Time history of the loss function during the adaptive learning process.

applied only as post-processing limits to maintain physical plausibility and numerical stability, while the theoretical control law itself remains unconstrained. A visual comparison reveals that the AI-augmented approach reconstructs the plume distribution more accurately. Without AI, agents tend to oversample near high-density regions and become trapped in local minima due to the absence of an escape mechanism. The proposed adaptive variance mechanism mitigates this by increasing the virtual uncertainty of unvisited samples, encouraging exploration of underrepresented regions. Consequently, all plume sources are successfully detected, and the final sample distribution aligns closely with the ground truth.

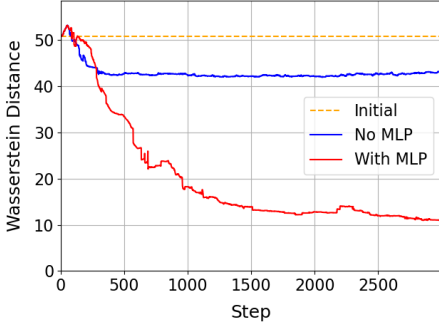


Fig. 3. Wasserstein distance comparison with GT: initial (orange); no MLP (blue); AI-augmented (red).

The learning behavior of the MLP-AdaptiveStd is shown in Fig. 2(d). The network is updated every ten control steps over a total of 3000 control steps. The loss fluctuates within a bounded range of approximately $[1.4\text{--}2.4] \times 10^{-3}$, reflecting the dynamic nature of online adaptation. Since MLP-AdaptiveStd continuously updates to align with the evolving virtual variance fields rather than a static target, the regularization loss does not decrease monotonically. Intermittent communication and local sample merging cause distribution shifts, yet the bounded oscillation of the loss indicates that the adaptation remains stable and well-regulated under decentralized operation.

The Wasserstein distance comparison in Fig. 3 quantitatively evaluates the distributional alignment between the reconstructed and ground-truth densities. The flat orange line corresponds to the static initial reference, while the blue and red curves represent D²OC without and with MLP, respectively. As shown in Fig. 3 and consistent with Theorem 2, the Wasserstein distance in the AI-augmented D²OC case shows an overall decreasing trend with minor fluctuations, whereas the non-MLP baseline remains nearly stagnant. The simulation results confirm this theoretical behavior, showing that the AI-augmented version consistently maintains a smaller Wasserstein distance, indicating more stable convergence and higher reconstruction fidelity under sensing and communication constraints.

7. CONCLUSION

This paper presented an AI-augmented D²OC framework for decentralized multi-agent mapping under sensing and communication constraints. By integrating dual-MLP inference into D²OC, each agent adaptively prioritized exploration based on predicted mean and uncertainty, enabling efficient reconstruction of complex spatial distributions without centralized coordination. The proposed framework preserves the theoretical convergence guarantees of D²OC under the Wasserstein metric while improving robustness to measurement noise, dynamic sample renewal, and intermittent communication. Simulation results demonstrated that the proposed method achieved lower steady-state Wasserstein distance and higher map fidelity than conventional decentralized approaches, confirming improved global consistency in spatial coverage. Future work will extend the framework to dynamic environments, heterogeneous agent systems, and real-world UAV experiments for large-scale environmental monitoring and disaster response.

REFERENCES

Afrazi, M., Seo, S., and Lee, K. (2025). Enhanced density-driven control of multi-agent uav systems for efficient victim detection in large-scale disaster scenarios. *International Journal of Control, Automation and Systems*, 23(9), 2728–2742.

Bandyopadhyay, S., Chung, S.J., and Hadaegh, F.Y. (2017). Probabilistic and distributed control of a large-scale swarm of autonomous agents. *IEEE Transactions on Robotics*, 33(5), 1103–1123.

Binney, J., Krause, A., and Sukhatme, G.S. (2013). Optimizing waypoints for monitoring spatiotemporal phenomena. *The International Journal of Robotics Research*, 32(8), 873–888.

Binney, J. and Sukhatme, G.S. (2012). Branch and bound for informative path planning. In *2012 IEEE international conference on robotics and automation*, 2147–2154. IEEE.

Gkouletsos, D., Iannelli, A., de Badyn, M.H., and Lygeros, J. (2021). Decentralized trajectory optimization for multi-agent ergodic exploration. *IEEE Robotics and Automation Letters*, 6(4), 6329–6336.

Hollinger, G.A. and Sukhatme, G.S. (2014). Sampling-based robotic information gathering algorithms. *The International Journal of Robotics Research*, 33(9), 1271–1287.

Julian, B.J., Angermann, M., Schwager, M., and Rus, D. (2012). Distributed robotic sensor networks: An information-theoretic approach. *The International Journal of Robotics Research*, 31(10), 1134–1154.

Kabir, R.H. and Lee, K. (2021). Wildlife monitoring using a multi-uav system with optimal transport theory. *Applied Sciences*, 11(9), 4070.

Krishnan, V. and Martínez, S. (2025). Distributed online optimization for multi-agent optimal transport. *Automatica*, 171, 111880.

Li, J., Zhou, J., Xiong, Y., Chen, X., and Chakrabarti, C. (2022). An adjustable farthest point sampling method for approximately-sorted point cloud data. In *2022 IEEE workshop on signal processing systems (SiPS)*, 1–6. IEEE.

Mathew, G. and Mezić, I. (2011). Metrics for ergodicity and design of ergodic dynamics for multi-agent systems. *Physica D: Nonlinear Phenomena*, 240(4-5), 432–442.

Moreau, L. (2005). Stability of multiagent systems with time-dependent communication links. *IEEE Transactions on automatic control*, 50(2), 169–182.

Rouet-Leduc, B. and Hulbert, C. (2024). Automatic detection of methane emissions in multispectral satellite imagery using a vision transformer. *Nature Communications*, 15(1), 3801.

Seo, S. and Lee, K. (2025a). Density-driven multidrone coordination for efficient farm coverage and management in smart agriculture. *IEEE Transactions on Control Systems Technology*.

Seo, S. and Lee, K. (2025b). Density-driven optimal control for efficient and collaborative multi-agent non-uniform coverage. *IEEE Transactions on Systems, Man, and Cybernetics: Systems*.

Shaw, J.T., Shah, A., Yong, H., and Allen, G. (2021). Methods for quantifying methane emissions using unmanned aerial vehicles: A review. *Philosophical Transactions of the Royal Society A*, 379(2210), 20200450.